Temperature dependence of commercial 4H-SiC UV Schottky photodiodes for X-ray detection and spectroscopy

Article (Published Version)

Nuclear Instruments and Methods in Physics Research A 859 (2017) 76–82

Contents lists available at ScienceDirect

Nuclear Instruments and Methods in Physics Research A

journal homepage: www.elsevier.com/locate/nima

Temperature dependence of commercial 4H-SiC UV Schottky photodiodes for X-ray detection and spectroscopy

S. Zhao[a,*], G. Lioliou[a], A.M. Barnett[a]

[a] Semiconductor Materials and Devices Laboratory, School of Engineering and Informatics, University of Sussex, Falmer, Brighton BN1 9QT, UK

ARTICLE INFO

Keywords:
X-ray detector
Photodiode
Silicon carbide
COTS
Commercial off the shelf
Temperature dependence

ABSTRACT

Two commercial-off-the-shelf (COTS) 4H-SiC UV photodiodes have been investigated for their suitability as low-cost high temperature tolerant X-ray detectors. Electrical characterisation of the photodiodes which had different active areas (0.06 mm^2 and 0.5 mm^2) is reported over the temperature range 0 °C to 140 °C together with measurements of the X-ray photocurrents generated when the detectors were illuminated with an ^{55}Fe radioisotope X-ray source. The 0.06 mm^2 photodiode was also investigated as a photon counting spectroscopic X-ray detector across the temperature range 0 °C to 100 °C. The depletion widths (at 120 V reverse bias) of the two diodes were found to be 2.3 μm and 4.5 μm, for the 0.06 mm^2 and 0.5 mm^2 detectors respectively, at 140 °C. Both devices had low leakage currents (< 10 pA) at temperatures ≤40 °C even at high electric field strengths (500 kV/cm for 0.06 mm^2 diode; 267 kV/cm for 0.5 mm^2 diode). At 140 °C and similar field strengths (514 kV/cm for 0.06 mm^2 diode; 269 kV/cm for 0.5 mm^2 diode), the leakage currents of both diodes were < 2 nA (corresponding to leakage current densities of 2.4 μA/cm^2 and 0.3 μA/cm^2 for each diode respectively). The results demonstrated that both devices could function as current mode detectors of soft X-rays at the temperatures < 80 °C and that when coupled to a low noise charge sensitive preamplifier, the smaller diode functioned as a photon counting spectroscopic X-ray detector at temperatures ≤100 °C with modest energy resolution (1.6 keV FWHM at 5.9 keV at 0 °C; 2.6 keV FWHM at 5.9 keV at 100 °C). Due to their temperature tolerance, wide commercial availability, and the radiation hardness of SiC, such detectors are expected to find utility in future low-cost nanosatellite (cubesat) missions and cost-sensitive industrial applications.

1. Introduction

Recently, many materials have been investigated for use in high temperature photon counting X-ray spectrometers. Compared with narrower bandgap materials, e.g. Si (E_g =1.12 eV) [1], wide bandgap materials, e.g. GaAs [2,3] (E_g =1.42 eV [4]), $Al_{0.8}Ga_{0.2}As$ [5] (E_g =2.09 eV [6]), 4H-SiC [7,8] (E_g =3.27 eV [9]), diamond [10] (E_g =5.5 eV [11]), and $Al_{0.52}In_{0.48}P$ [12,13] (E_g =2.43 eV [14]), can have better performance when operating at higher temperature. With high quality material available and well-developed fabrication technology, SiC detectors are especially attractive for such applications. Furthermore, they are also radiation tolerant [15], which can be essential in space science and exploration missions [16,17].

The performance of SiC Schottky diode X-ray detectors has been investigated extensively over the past 15 years, with the first measurements of X-ray detection with Schottky junctions on epitaxial SiC being reported in 2001 [18]. SiC was first shown to be suitable for X-ray detection and spectroscopy at high temperatures (100 °C) in 2002 [19], a more detailed study of the same work with improved results was subsequently reported in 2004 [20]. More recently, results have been reported showing energy resolutions as good as 233 eV FWHM at 5.9 keV at 100 °C using ultra-low-noise preamplifier electronics and high-quality semiconductor material [21]. Moreover, the ultra-low leakage current achievable with SiC detectors has stimulated the development of ultra-low-noise charge-sensitive preamplifiers [22]. Whilst such results are superb and demonstrate the suitability and high technology readiness level of the material and the excellent quality of the researchers' preamplifiers many researchers may not have access to such facilities, yet still desire to make photon counting X-ray spectrometers using low-cost commercial-off-the-shelf components for applications such as university-led Cubesat missions and industrial monitoring devices.

Previously, results have been reported showing that commercial-off-the-shelf 4H-SiC photodiodes (sold as UV photodetectors by a standard electronics retailer) could be repurposed as X-ray detectors for use at room temperature [23]. Here, the electrical and X-ray

* Corresponding author.
E-mail address: Shifan.Zhao@sussex.ac.uk (S. Zhao).

http://dx.doi.org/10.1016/j.nima.2017.04.008
Received 20 January 2017; Received in revised form 5 April 2017; Accepted 5 April 2017
Available online 07 April 2017

detection characterisation of these detectors are reported at temperatures up to 140 °C.

2. 4H-SiC UV photodiodes

SiC UV Schottky photodiodes of two different active areas (0.06 mm^2 and 0.5 mm^2) were purchased from a standard electronics retailer. The photodiodes were manufactured by sglux SolGel Technologies GmbH, Berlin, Germany [24,25]. The UV windows of the TO-18 packages were removed as Ref. [23]. At a temperature of 24 °C, the capacitances of 0.06 mm^2 photodiode and 0.5 mm^2 photodiode (excluding package, 0.67 pF) were 2.1 pF and 9.8 pF, respectively, at 100 V reverse bias. The leakage currents were 0.2 pA and 6 pA, respectively, at 100 V reverse bias [23]. The calculated depletion widths were 2.5 μm (0.06 mm^2 diode) and 4.5 μm (0.5 mm^2 diode) based on the devices' capacitances at 150 V reverse bias.

3. Experiments

3.1. Electrical characterisation

3.1.1. Capacitance-voltage measurements

The capacitances of the two photodiodes were measured as functions of applied reverse bias across the temperature range 0 °C to 140 °C. In turn, each photodiode was installed in a TAS Micro MT climatic cabinet for temperature control. The capacitance measurements were made using an HP 4275 A Multi Frequency LCR meter with an AC test signal of 60 mV rms magnitude and 1 MHz frequency; a Keithley 6487 Picoammeter/Voltage source was used as the external voltage supply. Measurements of the devices' capacitances as functions of temperature were made from 140 °C to 0 °C, with a decrement step size of 20 °C. To ensure thermal equilibrium, the devices were allowed to stabilise at each temperature for 30 min before measurements were started at each temperature. The devices were reverse biased from 0 V to 120 V, in 1 V increments. National Instruments Labview software was used to automate the measurements.

Since the devices were supplied packaged, in order to separate the capacitances of the diodes from the capacitances of the packaging, two sacrificial packaged devices (one for the 0.06 mm^2 photodiode; one for the 0.5 mm^2 photodiode), had their bond wires intentionally broken. The capacitances of the packages with the dice still mounted in each package, but the bond wires removed, were measured across the temperature range using the same procedure as was outlined above. The capacitances of the packages were independent of applied bias but dependent on temperature. The results are presented in Fig. 1.

To determine the capacitances of the photodiodes themselves, the

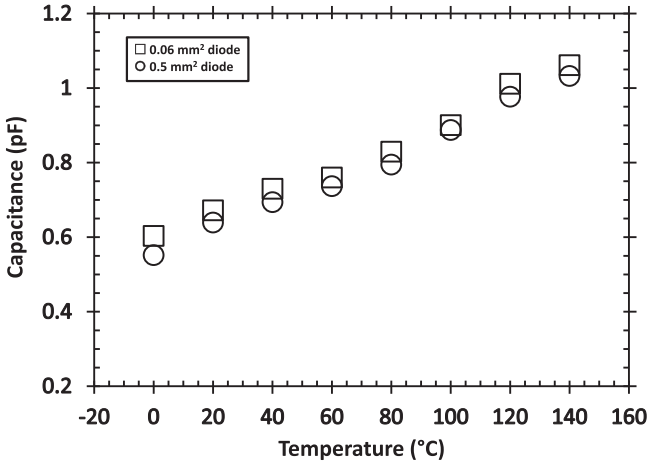

Fig. 1. Measured capacitances of the detectors' packages as functions of temperature for the 0.06 mm^2 diode (open squares) and 0.5 mm^2 diode (open circles).

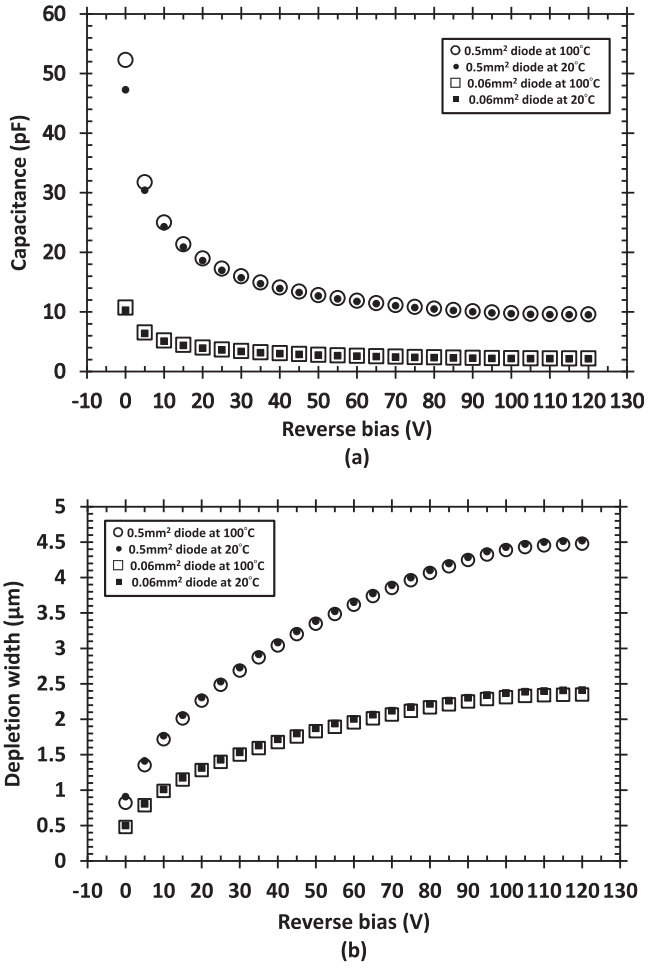

Fig. 2. (a) Measured capacitances of 0.5 mm^2 (open circles 100 °C and solid circles 20 °C) and 0.06 mm^2 (open squares 100 °C and solid squares 20 °C) photodiode as functions of applied reverse bias. (b) Calculated depletion width of 0.5 mm^2 (open circles 100 °C and solid circles 20 °C) and 0.06 mm^2 (open squares 100 °C and solid squares 20 °C) photodiode as functions of applied reverse bias.

package capacitances (presented in Fig. 1) were subtracted from the capacitances measured with the photodiodes wire-bonded. The device capacitances as subsequently determined, and the depletion width of each diode implied by those capacitances are shown in Fig. 2, for the 0.06 mm^2 and the 0.5 mm^2 photodiodes at the temperature of 20 °C and 100 °C, respectively. Fig. 2 showed the 0.06 mm^2 diode has been fully depleted (2.30 ± 0.03) μm at more than 90 V reverse bias and the 0.5 mm^2 diode has been fully depleted (4.49 ± 0.02) μm at the reverse bias of more than 110 V. Two contributors can explain the recorded increases in the capacitances of these devices with increased temperature. One is an increase in charge density in the depletion layer with increased temperature; a similar effect was previously found in abrupt p^+-n diodes and attributed to an effect where the trap density with an energy level near the centre of the bandgap contributed to a measured increase in capacitance with temperature. Thus, there may have been an increase in the excess donor concentration (N_d) with temperature, with the capacitance of the device at each temperature being expressed by,

$$C = \sqrt{\frac{q\epsilon_s N_d}{2(V_D - V)}} \quad (1)$$

where q is the elementary charge, ϵ_s is semiconductor permittivity, V_D is the diffusion voltage, and V is the external bias voltage [26]. The other contributor is the progressive ionization of previously non-ionised donors in a thin region around the depletion layer with

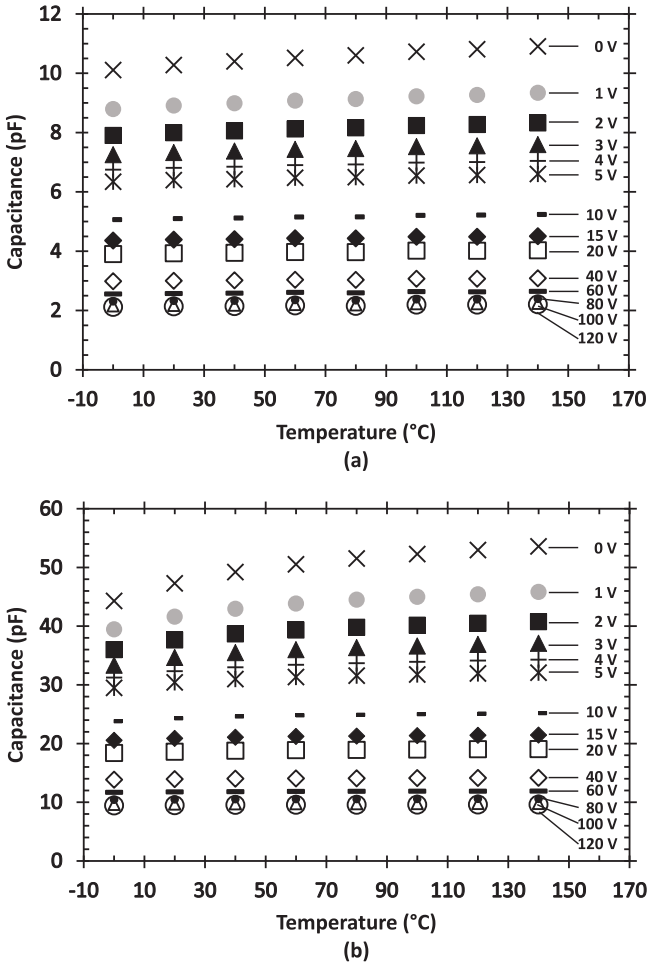

Fig. 3. Capacitance as a function of temperature for (a) the 0.06 mm^2 diode and (b) the 0.5 mm^2 diode in the temperature range of 0 °C to 140 °C at varying reverse biases, 0 V (× symbols), 1 V (grey circles), 2 V (dark squares), 3 V (dark triangles), 4 V (+ symbols), 5 V (stars), 10 V (short dashes), 15 V (dark diamonds), 20 V (open squares), 40 V (open diamonds), 60 V (dashes), 80 V (black circles), 100 V (open triangles), 120 V (open circles).

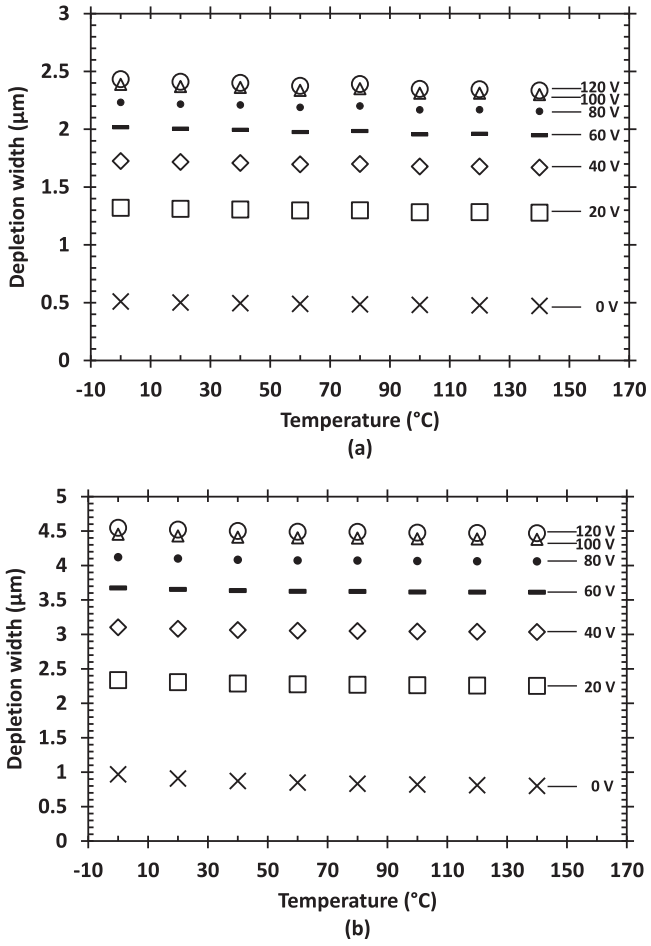

Fig. 4. Calculated depletion width as a function of temperature for (a) 0.06 mm^2 diode and (b) 0.5 mm^2 diode in the temperature range of 0 °C to 140 °C at seven reverse biases 0 V (× symbols), 20 V (open squares), 40 V (open diamonds), 60 V (dashes), 80 V (dark circles), 100 V (open triangles), 120 V (open circles).

increasing temperature [27].

The temperature dependence of each diode's capacitance and depletion width became less significant at high reverse biases (> 20 V), as shown in Figs. 3 and 4. This may be explained by the lower the ratio between the thickness of the thin region near the depletion layer with non-ionized donors, and the thickness of the depletion layer at high reverse biases [27]. The capacitance temperature coefficient (from 0 °C to 140 °C) was found to be 0.3 fF /°C and 0.1 fF/°C for the 0.06 mm^2 photodiode and 0.5 mm^2 by the measured capacitances at 120 V reverse bias. The thicknesses of the depletion widths of the 0.06 mm^2 and 0.5 mm^2 photodiodes were found to be 2.34 ± 0.03 µm and 4.47 ± 0.02 µm, respectively, both at 120 V reverse bias and 140 °C.

3.1.2. Current-voltage measurements

The ultra-low leakage currents of SiC junctions are one of key beneficial features of SiC detectors [28]. The leakage currents of the two photodiodes were measured each in turn as functions of applied reverse bias from 0 V to 120 V in 1 V increments, at temperatures from 140 °C to 40 °C, in steps of 20 °C. The devices were installed in a TAS Micro MT climatic cabinet for temperature control. A Keithley 6487 Picoammeter/Voltage Source was used to bias the devices. National Instruments Labview software was used to automate the measurements. To ensure thermal equilibrium, each device was allowed 30 mins to stabilise at each temperature before measurements began.

The results showed that the dark current was increased at high temperatures for all applied bias, as shown in Fig. 5. The dark currents of both devices at the same reverse bias and temperature were similar because the packages of the diodes (rather than the semiconductor junctions) are the dominant source of leakage current in the system. The dark currents of the 0.06 mm^2 photodiode and the 0.5 mm^2 photodiode at 120 V reverse bias were both found to be (0.2 ± 0.4) pA at 40 °C, and (1.454 ± 0.005) nA and (1.537 ± 0.005) nA, respectively, at 140 °C. At temperatures < 40 °C, the leakage currents of the devices were too small to measure with the experimental apparatus used. It is interesting to compare the high temperature leakage currents of the present devices with high-quality custom-made X-ray photodiodes. The leakage current densities of the 0.06 mm^2 and 0.5 mm^2 photodiodes at 100 °C were 7.9 ± 0.7 nA/cm^2 and 2.6 ± 0.1 nA/cm^2, respectively, at applied electric fields of 101 kV/cm. These are comparable to previously reported custom-made SiC X-ray detectors of high quality (e.g. 1 nA/cm^2 with mean electric field of 103 kV/cm at 107 °C [21]), and better than some custom-made GaAs X-ray photodiodes at 100 °C (e.g. 20 $\mu A/cm^2$ with an electric field of 21.4 kV/cm [2]).

3.2. Current mode X-ray measurements

An ^{55}Fe radioisotope X-ray source (Mn Kα =5.9 keV; Mn Kβ =6.5 keV; activity =231 MBq; active area =28.27 mm^2) was placed 2 mm above the diodes to investigate the soft X-ray response of the diodes at varying temperatures. The measured photocurrents (the illuminated current with the previously measured dark current sub-

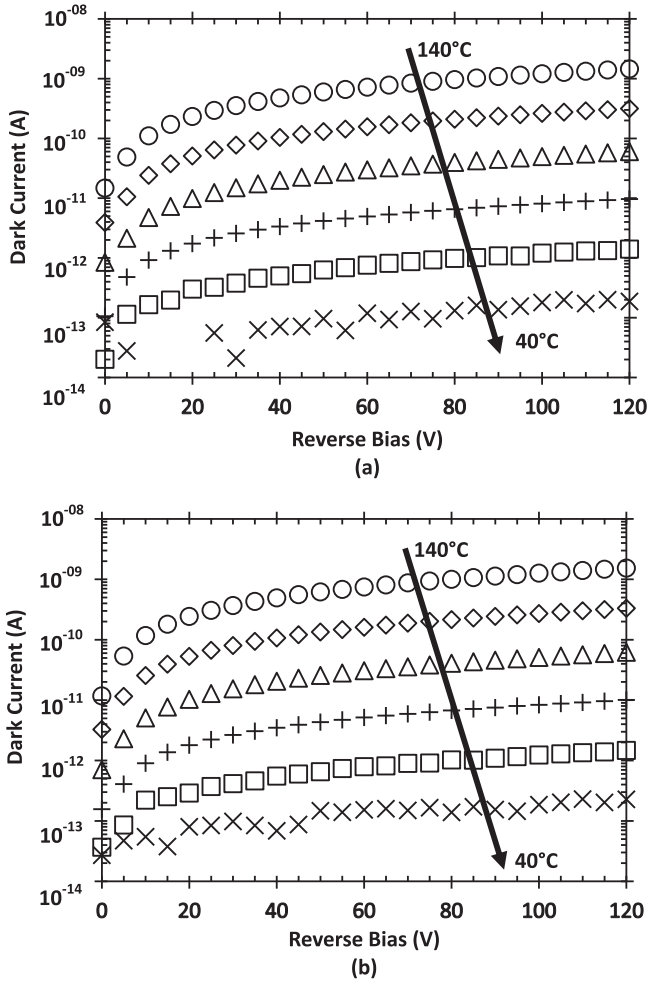

Fig. 5. Leakage current as a function of temperature for (a) 0.06 mm^2 diode and (b) 0.5 mm^2 diode in the range of 40 °C to 140 °C at varying reverse biases.

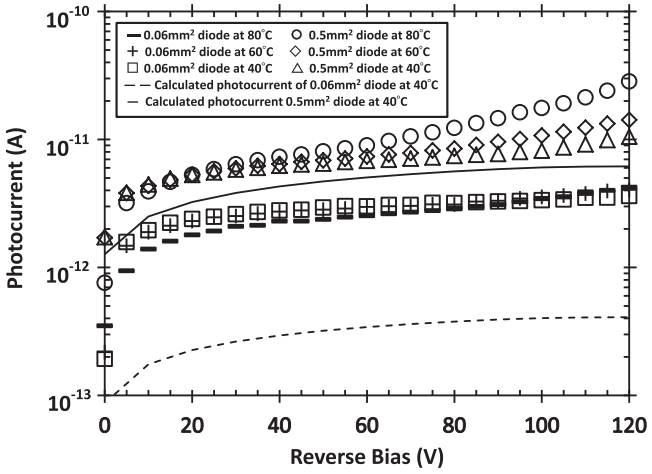

Fig. 6. Photocurrent as a function of applied reverse bias for the 0.06 mm^2 (80 °C, open squares; 60 °C, + symbols; 40 °C, dashes) and 0.5 mm^2 (80 °C, open circles; 60 °C, open diamonds; 40 °C, open triangles) diode. Expected photocurrents for the 0.06 mm^2 diode (dash line), and 0.5 mm^2 diode (solid line) at 40 °C.

tracted) as functions of applied reverse bias for the 0.06 mm^2 and 0.5 mm^2 devices are presented in Fig. 6, at temperatures from 40 °C to 80 °C. At temperatures above 80 °C, the photocurrents of both devices could not be measured due to the high dark currents of the devices at temperatures > 80 °C relative to the comparatively small photocurrent, and the sensitivity of the Keithley 6487 Picoammeter/Voltage Source. The photocurrents of the 0.06 mm^2 photodiode and the 0.5 mm^2 photodiodes were found to be (4.2 ± 0.2) pA and (28.4 ± 1.3) pA at 80 °C and 120 V reverse bias, respectively.

In order to calculate the expected photocurrents for these diodes, assuming an electron-hole pair creation energy for SiC =7.8 eV [29], and given the quantum efficiencies of the devices computed from the calculated depletion widths at 120 V reverse bias (2.4 μm for 0.06 mm^2 diode; 4.5 μm for 0.5 mm^2 diode) at 40 °C, as well as the activity geometry of the ^{55}Fe radioisotope X-ray source, and its relative X-ray emission probabilities (Mn Kα 5.9 keV =0.245; Mn Kβ 6.49 keV =0.0338 [30]), the calculated expected photocurrents at 120 V reverse bias of the 0.06 mm^2 diode and 0.5 mm^2 diode were 0.41 pA and 6.17 pA, respectively. These values assume that only charge created in the depletion region contributed to the signal and that there was 100% charge collection efficiency [15,31].

Interestingly, the expected photocurrents were much smaller than the measured photocurrents of the 0.06 mm^2 photodiode and 0.5 mm^2 photodiode at 120 V and 40 °C. The largest measured photocurrents of the 0.06 mm^2 photodiode (4.23 ± 0.41) pA and 0.5 mm^2 photodiode (28.41 ± 0.49) pA were obtained at 120 V reverse bias and 80 °C.

The apparent greater than expected photocurrents are possibly due to several factors. Firstly, contribution from electron-hole pairs generated around the edge of the depletion region leading to collection of charge carriers from a greater volume than assumed will have augmented the signal (i.e. at least some carriers generated outside of the depletion region contributed to the detected signal). If this was the sole influencing effect, the detected photocurrents imply that the active thicknesses of the detectors were 8.1 μm for the 0.5 mm^2 photodiode (i.e. 3.6 μm beyond the depletion region, which is conceivable), and 34.5 μm for the 0.06 mm^2 photodiode (which is too large to be reasonable). Secondly, there may also have been some contribution from impact ionization [32]; however, it should be noted that the devices were operated at a lower electric field strength (0.5 MV/cm, assuming a uniform field across the depletion layer) than that at which avalanche multiplication in 4H-SiC has been previously reported to start to play a role in current generation (0.9 MV/cm [32]). Thus, it is hypothesized that if there was impact ionization, it would have been due to localised material defects in the detector leading to localised regions of high electric field strength, rather than multiplication across the whole of the depletion layer. The electric field-dependence of the photocurrent of the 0.5 mm^2 diode became significant at high reverse bias (> 60 V) which is consistent with increased avalanche multiplication, which is also field-dependent. However, the effects were found to be more significant at higher temperatures. Since the temperature dependences of the impact ionization coefficients have previously been reported to be such that avalanche multiplication is reduced at higher temperatures as a result of increased phonon scattering [33,34], if an explanation of a contribution from impact ionization is correct, the mechanism or mechanisms causing the increased localised high electric field strength would have implied a stronger positive temperature coefficient than the negative temperature coefficient of the impact ionization coefficients. Thus, the exact nature of any contribution from impact ionization, if there was any, is still to be determined. A third explanation for the increasing photocurrent seen at high temperatures and reverse biases may be that under these conditions, the electron-hole pairs created by the X-ray photons increased the conductivity of the material such that a greater current from the bias supply could flow as a result of that decreased resistivity; this is thought to be unlikely given the relatively small amount of charge being created in the detectors by the X-ray photons per unit time. A final alternative explanation, is that the leakage current of the detectors may have been increased (relative to the prior leakage current measurements) if the detectors were disturbed when the ^{55}Fe radioisotope X-ray source was positioned above each of them. However, the utmost care was taken to avoid such disturbance. Use of a chopper wheel and lock-in amplifier may have enabled this influence to be

quantified or discounted, but our laboratory does not have such equipment at present.

3.3. Photon counting X-ray spectroscopy

The 0.06 mm^2 diode was connected to a custom-made low-noise charge-sensitive preamplifier with a wire-ended packaged 2N4416A silicon input JFET (capacitance =2 pF) and installed in a TAS Micro MT climatic cabinet for temperature control. The leg of the detector was directly soldered to the gate leg of the packaged JFET. An ORTEC 572A shaping amplifier and an ORTEC EASY-MCA 8k multi-channel analyser (MCA) were connected to the preamplifier. The photodiode was illuminated with the ^{55}Fe radioisotope X-ray source, which was placed 2 mm above the diode. The system was investigated at different shaping times (0.5 μs, 1 μs, 2 μs, 3 μs, 6 μs, and 10 μs) at each temperature (from 100 °C to 0 °C, with 20 °C steps) with the photodiode reverse biased at 100 V. Each spectrum had a live time limit of 60 s. The resulting spectra were calibrated in energy terms by using the position of the zero energy noise peak and the position of the fitted Kα at 5.9 keV for each spectrum as points of known energy on MCA's charge scale and assuming a linear variation of detected charge with energy. The energy resolution of the system at temperatures from 100 °C to 0 °C as quantified by the full width at half maximum (FWHM) of the 5.9 keV peak as functions of shaping time is shown in Fig. 7. At 100 °C, the photopeak could not be resolved from the zero energy noise peak at shaping times longer than 3 μs due to the large leakage current of the device (50 pA). At this temperature, the photopeak was also unresolved from the zero energy noise peak at a shaping time of 0.5 μs, due to the capacitance of the detector. However, a photopeak was resolved with the system at this temperature for shaping times of 1 μs (FWHM =2.68 keV), 2 μs (FWHM =2.62 keV), and 3 μs (FWHM =2.68 keV). The best energy resolution achieved with the system at each temperature is shown in Fig. 8. The energy resolutions at 5.9 keV at high temperature were not as good as some wide bandgap devices specifically designed for X-ray detection, e.g. GaAs mesa photodiodes (1.5 keV at 80 °C, area of 0.03 mm^2 [3]; 840 eV at 60 °C, area of 0.03 mm^2 [2]) and the best results obtained with custom-made SiC X-ray detectors (233 eV at 100 °C, area of 0.4 mm^2) [21], however, the FWHM of the device was comparable to $Al_{0.8}Ga_{0.2}As$ X-ray detectors at 80 °C (2.0 keV, area of 0.03 mm^2) [5]. Example spectra obtained with the present system at 0 °C and 60 °C are shown in Fig. 9.

3.4. Noise analysis

The energy resolution (FWHM) of a photodiode X-ray spectrometer is generally limited by the electronic noise of the detector and preamplifier, by the incomplete charge collection noise, and by the Fano noise [1]. The Fano noise is determined by the statistical fluctuations in the number of the electron-hole pairs created in the process of photon absorption [1]. The expected Fano-limited resolution (FWHM) of the devices examined here can be calculated as 160 eV at 5.9 keV, assuming the average energy consumed in the generation an electron-hole pair was 7.8 eV [29], and the Fano factor was 0.1 [21]. Clearly, the Fano noise was not the dominant noise contributor in the energy resolution of the system presented, rather the energy resolution was degraded by other noise sources.

The electronic noise arises from the series white noise, parallel white noise, 1/*f* noise, and the dielectric noise. A detailed explanation of the origin of each electronic noise can be found in Refs. [35,36]. The series white noise is proportional to the total capacitance at the preamplifier input (including the capacitances of the photodiode, input JFET of the preamplifier, feedback capacitor, and stray capacitances), it is inversely proportional to the shaping time. The parallel white noise is proportional to the leakage current of the photodiode and the input JFET, and it is proportional to the shaping time. The 1/*f* series noise is proportional to the total capacitance at the preamplifier input (including the capacitances of the photodiode, input JFET of the preamplifier, feedback capacitor, and stray capacitances), it is independent of the shaping time. Using the method given by Ref. [36], the capacitance and the leakage current of the input JFET can be estimated across the temperature range. A constant dielectric dissipation factor (dielectric

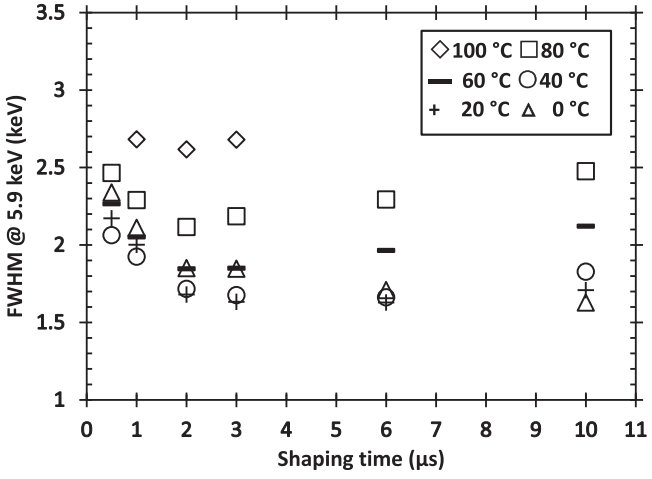

Fig. 7. Measured FWHM at 5.9 keV of 0.06 mm^2 as functions of applied shaping time at 100 V reverse bias.

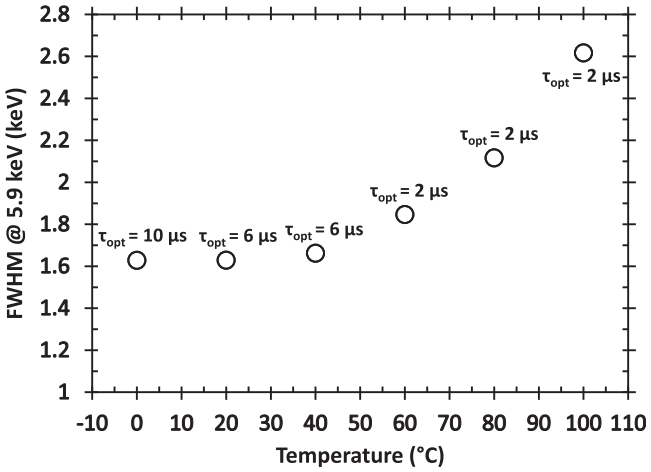

Fig. 8. The measured best energy resolution of the 0.06 mm^2 photodiode as a function of temperature at 100 V reverse bias. The shaping time which gave the best energy resolution at each temperature, τ_{opt} is indicated.

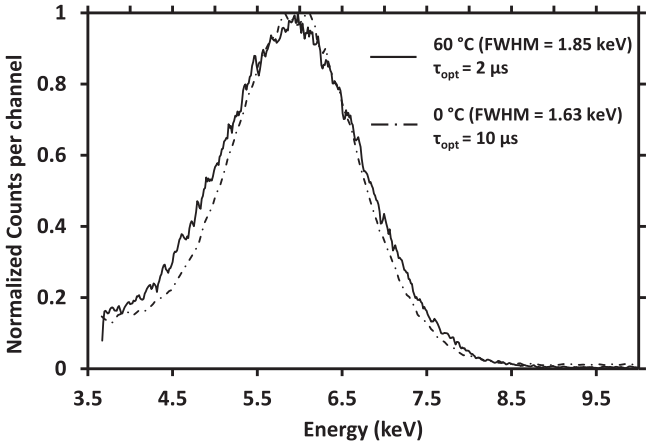

Fig. 9. ^{55}Fe X-ray spectrum obtained with 0.06 mm^2 photodiode at 100 V reverse bias at 0 °C and 60 °C.

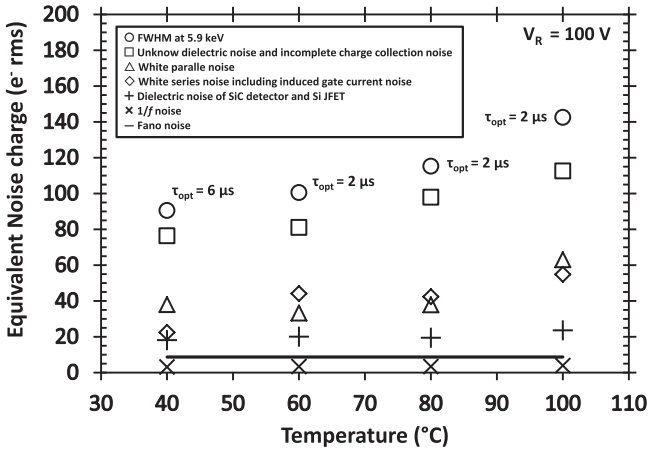

Fig. 10. Calculated components of noise contribution for the 0.06 mm^2 photodiode connected to the custom low-noise charge-sensitive preamplifier, at the optimal shaping time at each temperature. Measured FWHM at 5.9 keV (open circles), computed quadratic sum of known dielectric noise (SiC photodiode and Si input JFET) (+ symbols), computed quadratic sum of unknown dielectric noise and incomplete charge collection noise (open squares), white parallel noise (open triangles), white series noise including induced gate drain current noise (open diamonds), Fano noise (solid line), and $1/f$ series noise (× symbols).

loss tangent) of 4H-SiC (3.4×10^{-5} [37]) and Si (0.2×10^{-3} [38]) through the temperature range was assumed [37,39]. According to the estimated the leakage current and the capacitance of the input JFET and the measured leakage current and capacitance of the detector, parts of the electronic noise can be calculated (parallel white noise, series white noise, $1/f$ noise, and the known (i.e. readily calculable) dielectric noises of the SiC photodiode and the Si input JFET) at different temperatures. The calculated Fano noise, series white noise, parallel noise and the $1/f$ noise, the quadratic sum of known dielectric noise of the detector and the input JFET, and the quadratic sum of unknown dielectric noise and incomplete charge collection noise of the system are as shown in Fig. 10.

The unknown dielectric noise (and series white noise from unknown stray capacitances [1]) and any possible contribution from the incomplete charge collection noise cannot be directly calculated in this case. However, it is clear that the combined contributions of the unknown dielectric noise, noise from any unknown stray capacitances, and from any incomplete charge collection noise (where incomplete charge collection arises solely from carriers created in the substrate, not the epitaxial layers) are in combination the dominant noise for this system. The dielectric noise (and noise from stray capacitances) is thought to arise from dielectric materials of the capacitances and packages, by using a bare die JFET directly wire-bonded to the detector could be expected to descent the noise significantly [40]. The incomplete charge collection noise is related to the detector's charge diffusion and collection properties as well as to the trap density distribution in the detector [1].

The variation with temperature of the capacitance and the leakage current of the device in part determines the white series noise, $1/f$ noise, white parallel noise at each temperature. By changing the shaping time, the optimal energy resolution (within the limits of the range of shaping times available with the shaping amplifier used), that could be achieved at each temperature [40,41] was obtained. As shown in Fig. 8, the longest shaping time (τ=10 μs) was selected to achieve the optimal FWHM at low temperature (< 20 °C) because the leakage current (and hence parallel white noise) was small compared with the series white noise. On the contrary, shorter shaping times resulted in better energy resolutions at high temperature (> 40 °C) as the leakage current increased and the balance between the parallel white noise and series white noise changed.

4. Conclusions and future work

The electrical characterisation of different areas (0.06 mm^2 and 0.5 mm^2) of commercial 4H-SiC Schottky photodiodes at varying temperatures has been reported. The results of measurements of capacitance as functions of applied reverse bias at different temperatures showed the consistent capacitance in the investigated range of temperature at high reverse bias (≥100 V) for both photodiodes. The depletion widths for both devices were found to be 2.34 ± 0.03 μm and 4.47 ± 0.02 μm at the maximum investigated bias of 120 V at a temperature of 140 °C. Measurements of leakage current as functions of applied reverse bias at varying temperature showed the low leakage currents among these devices (< 10 pA) at 120 V reverse bias at the temperatures lower than 60 °C. The measured leakage currents of both devices were found to be < 2 nA at 120 V reverse bias (electric field strengths of 514 kV/cm and 269 kV/cm for 0.06 mm^2 photodiode and 0.5 mm^2 photodiode, respectively) at the highest investigated temperature (140 °C).

The performance of these devices as high temperature X-ray detectors was investigated by the measuring the generated photocurrent whilst the devices were illuminated by an ^{55}Fe radioisotope X-ray source, and by connecting the photodiode to a custom low-noise charge-sensitive preamplifier to investigate the device performance as a detector for photon counting X-ray spectroscopy. The largest photocurrents were found to be 4 pA with the 0.06 mm^2 photodiode and 28 pA with the 0.5 mm^2 photodiode at the highest investigated temperature (80 °C) and reverse bias (120 V). The 0.06 mm^2 detector functioned as photon counting spectroscopic X-rays detector with modest energy resolution (the FWHM at 5.9 keV was 2.6 keV at 100 V reverse bias at 100 °C). Although the energy resolution was not as good as many custom X-ray detectors, the results showed that the commercial off-the-shelf photodiode could be used for photon counting X-ray spectroscopy at high temperature. Noise analysis of the system was also presented. It showed that the dielectric noise and possible partial charge collection from the substrate were the dominant noise sources in the system in the investigated range of temperatures.

Acknowledgements

This work was in part supported by the Science and Technologies Facilities Council, United Kingdom, through grants ST/M004635/1 and ST/P001815/1 (University of Sussex, A.M.B., PI). A.M.B. acknowledges funding from the Leverhulme Trust in the form of a 2016 Philip Leverhulme Prize. G.L. acknowledges funding received from the University of Sussex, United Kingdom, in the form of a Ph.D. scholarship.

Authors' Data Statement: Data underlying this work are subject to commercially confidentiality. The Authors regret that they cannot grant public requests for further access to any data produced during the study.

References

[1] A. Owens, Compound Semiconductor Radiation Detectors, CRC Press, Boca Raton, 2012.
[2] G. Lioliou, X. Meng, J.S. Ng, A.M. Barnett, J. Appl. Phys. 119 (2016) 124507.
[3] A.M. Barnett, J.E. Lees, D.J. Bassford, J.S. Ng, C.H. Tan, N. Babazadeh, R.B. Gomes, Nucl. Instrum. Methods A 654 (2011) 336.
[4] G. Bertuccio, D. Maiocchi, J. Appl. Phys. 92 (2002) 1248.
[5] A.M. Barnett, D.J. Bassford, J.E. Lees, J.S. Ng, C.H. Tan, J.P.R. David, Nucl. Instrum. Methods A 621 (2010) 453.
[6] S. Adachi, J. Appl. Phys. 58 (1985) R1.
[7] J.B. Casady, R.W. Johnson, Solid-State Electron 39 (1996) 1409.
[8] G. Bertuccio, R. Casiraghi, A. Cetronio, C. Lanzieri, F. Nava, Electron. Lett. 40 (2004) 173.
[9] T. Seyller, Appl. Phys. A 85 (2006) 371.
[10] M. Tsubota, J.H. Kaneko, D. Miyazaki, T. Shimaoka, K. Ueno, T. Tadokoro, A. Chayahara, H. Watanabe, Y. Kato, S. Shikata, H. Kuwabara, Nucl. Instrum. Methods A 789 (2015) 50.

[11] S.F. Kozlov, E. Belcarz, M. Hage-Ali, R. Stuck, P. Siffert, Nucl. Instr. Meth. 117 (1974) 277.
[12] S. Butera, G. Lioliou, A.B. Krysa, A.M. Barnett, J. Appl. Phys. 120 (2016) 024502.
[13] A. Auckloo, J.S. Cheong, X. Meng, C.H. Tan, J.S. Ng, A. Krysa, R.C. Tozer, J.P.R. David, J. Instrum. 11 (2016) P03021.
[14] D.J. Mowbray, O.P. Kowalski, M. Hopkinson, M.S. Skolnick, J.P.R. David, Appl. Phys. Lett. 65 (1994) 213.
[15] F. Nava, G. Bertuccio, A. Cavallini, E. Vittone, Meas. Sci. Technol. 19 (2008) 102001.
[16] G.R. Gladstone, et al., Nature 415 (2002) 1000.
[17] G. Branduardi-Raymont, et al., A & A 424 (2004) 331.
[18] G. Bertuccio, R. Casiraghi, F. Nava, IEEE Trans. Nucl. Sci. 48 (2001) 232.
[19] G. Bertuccio, R. Casiraghi, E. Gatti, D. Maiocchi, F. Nava, C. Canali, A. Cetronio, C. Lanzieri, Mater. Sci. Forum 433– 436 (2003) 941.
[20] G. Bertuccio, R. Casiraghi, A. Cetronio, C. Lanzieri, F. Nava, Nucl. Instrum. Methods A 522 (2004) 413.
[21] G. Bertuccio, S. Caccia, D. Puglisi, D. Macera, Nucl. Instrum. Methods A 652 (2011) 193.
[22] G. Bertuccio, S. Caccia, Nucl. Instrum. Methods A 579 (2007) 243.
[23] S. Zhao, T. Gohil, G. Lioliou, A.M. Barnett, Nucl. Instrum. Methods A 830 (2016) 1.
[24] Anon, "Broadband SiC based UV photodiode A =0.06 mm2, SG01S-18," Rev.6.0, SGlux SolGel Technologies GmbH, Berlin, Germany. N.D.
[25] Anon, "Broadband SiC based UV photodiode A =0.50 mm2, SG01D–18," Rev.6.0, SGlux SolGel Technologies GmbH, Berlin, Germany. N.D.
[26] G. Gramberg, Solid-State Electron. 14 (1971) 1067.
[27] M. Mazzillo, A. Sciuto, G. Catania, F. Roccaforte, V. Raineri, IEEE Sens. J. 12 (2012) 1127.
[28] G. Bertuccio, et al., IEEE Trans. Nucl. Sci. 53 (4) (2006) 2421.
[29] G. Bertuccio, R. Casiraghi, IEEE Trans. Nucl. Sci. 50 (1) (2003) 175.
[30] U. Schötzig, Appl. Radiat. Isot. 53 (2000) 469.
[31] S.M. Sze, Semiconductor Devices Physics and Technology, Wiley, New York, 1985.
[32] S. Loh, B. Ng, J. David, S. Soloviev, H. Cha, IEEE Trans. Electron Dev. 55 (2008) 1984.
[33] R. Raghunathan, B.J. Baliga, Solid-State Electron 43 (1999) 199.
[34] H. Niwa, J. Suda, T. Kimoto, Mater. Sci. Forum 778–780 (2014) 461.
[35] G. Lioliou, A.M. Barnett, Nucl. Instrum. Methods A 801 (2015) 63.
[36] G. Bertuccio, A. Pullia, Rev. Sci. Instrum. 64 (1993) 3294.
[37] H.S. Jung, W.I. Yang, M.S. Cho, K.N. Joo, S.Y. Lee, Electron. Mater. Lett. 10 (2014) 541.
[38] B.G. Lowe, R.A. Sareen, Semiconductor X-Ray Detectors, CRC Press, Boca Raton, 2014.
[39] J.G. Hartnett, D. Mouneyrac, J. Krupka, J.M. le Floch, M.E. Tobar, D. Cros, J. Appl. Phys. 109 (2011) 064107.
[40] G. Bertuccio, A. Pullia, G. De Geronimo, Nucl. Instrum. Methods A 380 (1996) 301.
[41] A.M. Barnett, J.E. Lees, D.J. Bassford, J.S. Ng, Nucl. Instrum. Methods A 673 (2012) 10.